

## Article

# The Composition of Saturated Vapor over 1-Butyl-3-methylimidazolium Tetrafluoroborate Ionic Liquid: A Multi-Technique Study of the Vaporization Process

Anatoliy M. Dunaev \*, Vladimir B. Motalov and Lev S. Kudin

Research Institute of Thermodynamics and Kinetics, Ivanovo State University of Chemistry and Technology, 153000 Ivanovo, Russia; v.motalov@gmail.com (V.B.M.); LKudin@yandex.ru (L.S.K.)

\* Correspondence: amdunaev@ro.ru

**Abstract:** A multi-technique approach based on Knudsen effusion mass spectrometry, gas phase chromatography, mass spectrometry, NMR and IR spectroscopy, thermal analysis, and quantum-chemical calculations was used to study the evaporation of 1-butyl-3-methylimidazolium tetrafluoroborate (BMImBF<sub>4</sub>). The saturated vapor over BMImBF<sub>4</sub> was shown to have a complex composition which consisted of the neutral ion pairs (NIPs) [BMIm<sup>+</sup>][BF<sub>4</sub><sup>-</sup>], imidazole-2-ylidene C<sub>8</sub>N<sub>2</sub>H<sub>14</sub>BF<sub>3</sub>, 1-methylimidazole C<sub>4</sub>N<sub>2</sub>H<sub>6</sub>, 1-butene C<sub>4</sub>H<sub>8</sub>, hydrogen fluoride HF, and boron trifluoride BF<sub>3</sub>. The vapor composition strongly depends on the evaporation conditions, shifting from congruent evaporation in the form of NIP under Langmuir conditions (open surface) to primary evaporation in the form of decomposition products under equilibrium conditions (Knudsen cell). Decomposition into imidazole-2-ylidene and HF is preferred. The vapor composition of BMImBF<sub>4</sub> is temperature-dependent as well: the fraction ratio of [BMIm<sup>+</sup>][BF<sub>4</sub><sup>-</sup>] NIPs to decomposition products decreased by about a factor of three in the temperature range from 450 K to 510 K.

**Keywords:** ionic liquids; imidazolium; Knudsen effusion mass spectrometry; vapor composition; ylidene; imidazole



**Citation:** Dunaev, A.M.; Motalov, V.B.; Kudin, L.S. The Composition of Saturated Vapor over 1-Butyl-3-methylimidazolium Tetrafluoroborate Ionic Liquid: A Multi-Technique Study of the Vaporization Process. *Entropy* **2021**, *23*, 1478. <https://doi.org/10.3390/e23111478>

Academic Editors: Stefano Vecchio Cipriotti and Marilena Tolazzi

Received: 6 October 2021

Accepted: 29 October 2021

Published: 8 November 2021

**Publisher's Note:** MDPI stays neutral with regard to jurisdictional claims in published maps and institutional affiliations.



**Copyright:** © 2021 by the authors. Licensee MDPI, Basel, Switzerland. This article is an open access article distributed under the terms and conditions of the Creative Commons Attribution (CC BY) license (<https://creativecommons.org/licenses/by/4.0/>).

## 1. Introduction

In recent years, ionic liquids (ILs) have become one of the most fast-developing fields of chemistry. This keen interest is due to the unique combination of IL's properties, which includes the ability to dissolve organic, inorganic and polymer materials together with low vapor pressure at room temperatures [1]. Today, imidazolium-based ILs are the most investigated group of ionic liquids. They are distinguishable from others by quantifiable vapor pressures at 380–500 K and their relatively high decomposition temperatures [2]. This fact gives possibility to the use of these ILs in various heterophase processes such as distillation, chemical gas-phase deposition, etc. Therefore, the investigation of evaporation of the imidazolium-based ILs is particularly important.

It has been experimentally proven that many aprotic ILs evaporate congruently and that their vapors consist of neutral ion pairs (NIPs) [3–8]. However, evaporation of a number of aprotic ILs can be accompanied by a partial decomposition of the condensed phase. Some ILs, e.g., those containing chiral center, decompose while heating, and the decomposition processes prevail over evaporation [9]. Decomposition was marked for ILs with high electronegative anions (BF<sub>4</sub><sup>-</sup>, PF<sub>6</sub><sup>-</sup>, AsF<sub>6</sub><sup>-</sup>, SCN<sup>-</sup>, etc.) as well [10–12]. The 1-butyl-3-methylimidazolium tetrafluoroborate (BMImBF<sub>4</sub>) is a striking example of such a compound. As opposed to the alkylimidazolium ILs with NTf<sub>2</sub><sup>-</sup> anion having a simple vapor composition consisting exclusively of NIPs [6,13] at temperatures below the onset of decomposition, the vapor of BMImBF<sub>4</sub> contains many other components [14] at quite low temperatures, where any appreciable effects on thermal analysis curves are not evident. However, there is no consensus in the literature about this phenomenon: some

works [14–22] are concerned with the thermal behavior of BMImBF<sub>4</sub>, and conclude that the no thermal degradation of IL occurred, while at the same time the other authors [23–27] postulate the thermal decomposition of the investigated compound.

In a recent paper [10], the evaporation mechanism of BMImBF<sub>4</sub> was investigated using NMR analysis and mass spectrometry. The authors established the competitive vaporization and thermal decomposition of IL ruled by the sample surface area to volume ratio. The main decomposition route proposed in [10] was the formation of imidazol-2-ylidene (Figure 1a) through an Arduengo carbene [28] by cation-anion interaction. Previously, borane-substituted imidazol-2-ylidene was synthesized in vacuo from BMImBF<sub>4</sub> by Taylor et al. [29]. Some researchers [10,29] gave the NMR and mass spectra of pure ylidene and found that its vapor pressure was sufficiently higher than that of IL at the same temperatures. The evaporation of BMImBF<sub>4</sub> can also be accompanied by the formation of imidazoles [26,27]. These routes are the formation of 1-methylimidazole, 1-butene, HF, and BF<sub>3</sub> (Figure 1b), and 1-butylimidazole, fluoromethane, and BF<sub>3</sub> (Figure 1c). The pyrolysis-gas chromatography experiments [26,27] were carried out at much higher temperatures than that of decomposition (873 K and 823 K in refs. [26] and [27] respectively). The authors [26] concluded that the ratio between these two routes is close to 1:1. According to Ohtani et al. [27] the reaction with 1-methylimidazole formation is preferred. Formation of ethylimidazole from similar IL BMImPF<sub>6</sub> was observed by KEMS in Ref. [12]. Authors [12] noted the influence of orifice size on vapor composition: the larger the orifice, the larger the contribution of the BMImPF<sub>6</sub> vapor species. The investigation of ILs with cyano-functionalized anions [11,30], which are close to the object under study, showed one more degradation route by the intrinsic cyclization (Figure 1d) of the butyl group on the C1 atom.

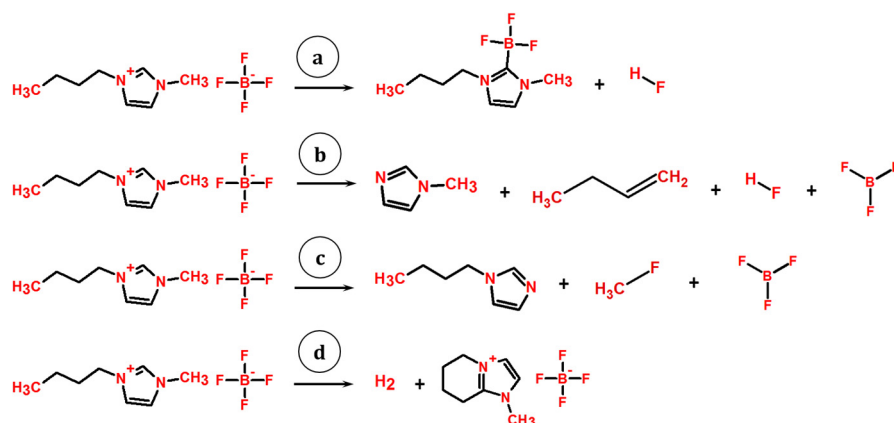


**Figure 1.** Schemes of BMImBF<sub>4</sub> decomposition with formation of imidazole-2-ylidene and HF (a); 1-methylimidazole, 1-butene, HF, and BF<sub>3</sub> (b); 1-butylimidazole, fluoromethane, and BF<sub>3</sub> (c); H<sub>2</sub> and bicyclic IL (d).

In a recent paper [31] the kinetic model of maximum operation temperature (MOT) was applied to BMImBF<sub>4</sub> IL. This model defines the temperature at which a mass loss of 1%, which can be attributed to thermal decomposition, occurs as a function of variable application time. It was found that MOT decreased exponentially with increasing application time (466 K at 1 h and 348 K at 1 year). The authors [31] also studied the vapor composition of BMImBF<sub>4</sub>. The decomposition products according to routes **b** and **c** (here and further designations as in Figure 1) were found in vapor. Additionally, the formation of imidazole and 1-butene from 1-butylimidazole was suggested and traces of imidazole were found.

Mass spectroscopy [10,14] revealed the partial decomposition of initial IL according to way **a** and did not find any traces of imidazoles. It should be noted that in a recent paper [12] with the analogous BMImPF<sub>6</sub> IL, none of the ylidenes were registered, whereas the ethylimidazole was observed in vapor.

The available thermodynamic studies of BMImBF<sub>4</sub> were carried out without any analysis of the gas phase composition [17–19]. As a result, the vapor pressures of BMImBF<sub>4</sub> obtained in these works disagree by some orders of magnitude. Therefore, the comprehensive analysis of the vapor composition of the mentioned group of ILs is mandatory in thermodynamic investigations.

This work is a multi-technique study of the BMImBF<sub>4</sub> evaporation carried out with the use of Knudsen effusion mass spectrometry (KEMS), IR and NMR spectroscopy, thermal analysis, gas-phase chromatography–mass spectrometry (GCMS), and quantum chemical modelling. The main goals are to determine the composition of saturated vapor over BMImBF<sub>4</sub> and to clarify the routes of thermal decomposition while heating.

## 2. Experimental

Thermal analysis of the samples (98% purity, Sigma-Aldrich, St. Louis, MO, USA) was performed on a synchronous thermal analysis instrument Netzsch STA 449 F3 Jupiter (NETZSCH-Gerätebau, Selb, Germany) in the temperature range of 20–500 °C at a speed of 5 °C/min in nitrogen atmosphere. The device has high sensitivity with a resolution of 0.1 µg. In parallel with the data on weight loss, the temperature dependences of the thermal effects were recorded at the resolution of 1 µW.

IR spectroscopic measurements were carried out on a Bruker Tensor 27 (Bruker AXS, Madison, WI, USA) spectrometer with Fourier transform. The operating frequency range was 370–4000 cm<sup>−1</sup> with a resolution of 1 cm<sup>−1</sup>. The instrument makes it possible to obtain both the spectra of the condensed phases and the temperature dependences of the absorption for the gas phase.

NMR spectra <sup>1</sup>H, <sup>13</sup>C, <sup>11</sup>B, <sup>15</sup>N in DMSO-*d*<sub>6</sub> at *T* = 22 °C and *T* = 70 °C were recorded by a Bruker Avance 500 (Bruker AXS, Madison, US) spectrometer with 5 mm TBI 1H/31P/D-BB z-GRD sensor. A working frequency for <sup>1</sup>H was 500.17 MHz, <sup>13</sup>C—125.77 MHz, <sup>11</sup>B—160.47 MHz, <sup>15</sup>N—50.68 MHz. <sup>13</sup>C NMR spectra were obtained using broadband proton decoupling (WALTZ 16). <sup>15</sup>N chemical shift measurements were made based on two-dimensional HMBC <sup>15</sup>N-<sup>1</sup>H spectra. The solvent signal (DMSO-*d*<sub>6</sub>) was used as a reference for <sup>1</sup>H, <sup>13</sup>C spectra; BF<sub>3</sub>OEt<sub>2</sub> was used for <sup>11</sup>B; nitromethane was used for <sup>15</sup>N. The signal assignment in spectra of objects under study was performed on a base of literature data [32–36] and NMR-prediction instruments.

A magnetic sector mass spectrometer MI1201 (PO “Electron”, Sumy, Ukraine) coupled with a Knudsen cell was used for vapor analysis. Neutral vapor species were studied using a combined ion source operating in electron-ionization (EI) mode. A detailed description of the apparatus is given elsewhere [37–39].

The GCMS experiments were carried out on a Shimadzu GCMS QP2010 Ultra (Shimadzu, Kyoto, Japan). Each sample was analyzed in programmable mode: a column temperature was kept at 100 °C during 5 min, after that the sample was heated with a speed of 5 °C/min up to 250 °C. Two types of columns were used: polar (Agilent DB-17MS capillary column) and non-polar (Zebron ZB-5MS capillary column).

## 3. Computational Details

The molecular structure of conformers of the neutral ionic pair [C<sub>4</sub>mim<sup>+</sup>][BF<sub>4</sub><sup>−</sup>] and the cation [C<sub>4</sub>mim<sup>+</sup>] has been studied by the density functional theory method (pure B3LYP, B3LYP with D3 version of Grimme’s dispersion [40], long-range-corrected version of B3LYP using the Coulomb-attenuating CAM-B3LYP functional [41], as well as hybrid functional of Truhlar and Zhao M06 [42]) with the use of the Dunning’s correlation consistent triple basis sets cc-pVTZ [43]. All calculations were carried out using the Gaussian 09 package [44]. Comparison of IR spectra of computed molecules with experiment revealed a more accurate description of molecular structure by the CAM-B3LYP functional, which is used in all calculations.

The nine most energetically preferable conformers of the [BMim<sup>+</sup>] cation were selected on a basis of conformational analysis. The structures of the BMImBF<sub>4</sub> conformers are

depicted in Figure S1 (see Supplementary Materials). Each cation conformer can exist together with the  $[\text{BF}_4^-]$  anion in two forms: “close” (denoted as “a”) and “open” (denoted as “b”). The equilibrium mole fractions of the conformers in the temperature range of 300–500 K found on a basis of their relative free energies calculated by DFT are presented in Figure 2. The conformer 5a due to its lowest energy dominates in vapor at experimental conditions (400–500 K). Its structure is shown in Figure 3.

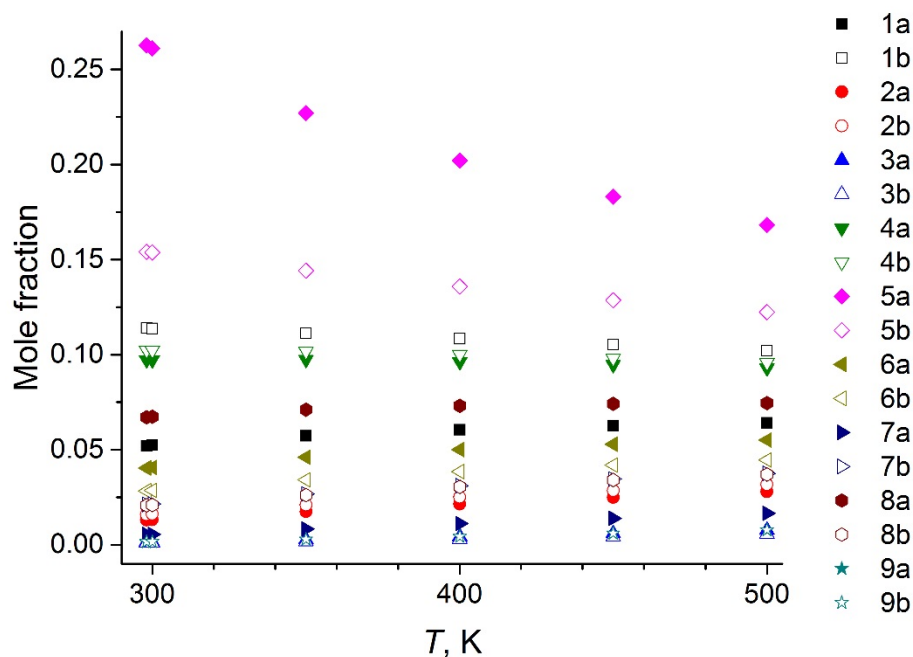


**Figure 2.** Computed vapor composition of the BMIImBF<sub>4</sub> conformers at 300–500 K (the structures corresponding to designations see in Supplementary Materials, Figure S1).

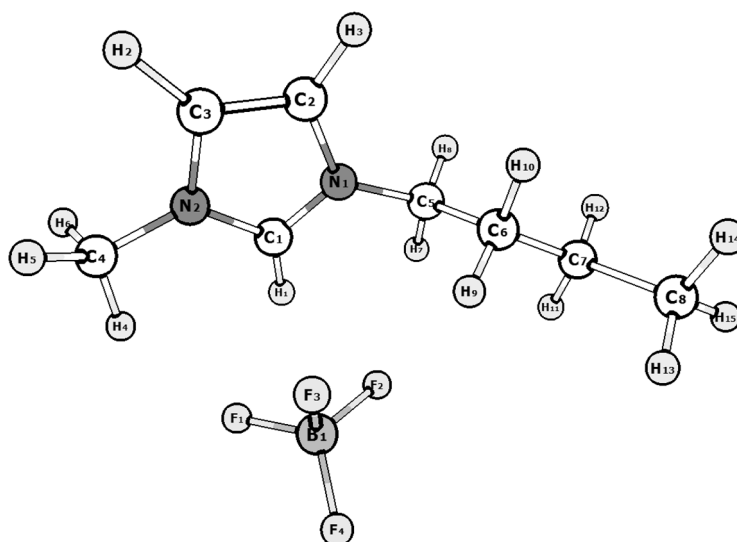


**Figure 3.** Structure of conformer 5a.

The IR spectra were modeled in the following manner: the intensities of vibrations of the conformers were multiplied by the corresponding mole fractions and are summarized through observed IR range (40–400  $\text{cm}^{-1}$ ).

## 4. Results

### 4.1. Thermal Analysis

The decomposition temperature  $T_{\text{dec}} = 685$  K was found as the average between the mass loss and DSC data (Figure 4). This value is quite close to that of 679 [31], 697 K [45], 712 K [46], 633–723 K [47] whereas the other literature data are somewhat lower: ~640 K [26], 653 K [48], and 634 K [23]. None of additional effects before decomposition were found.

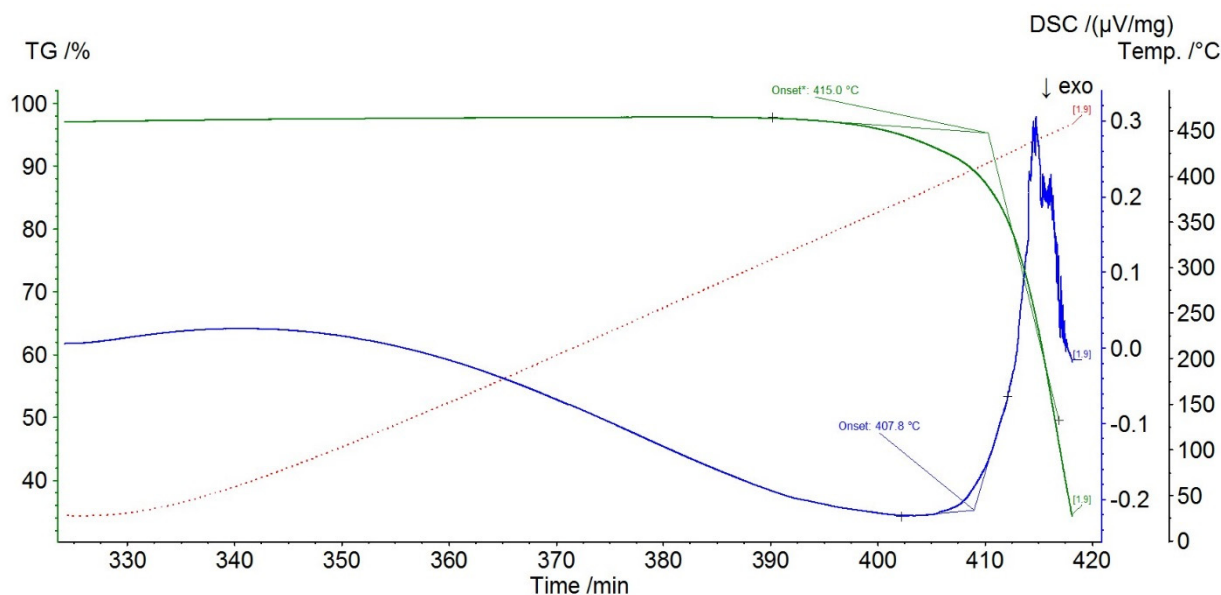


Figure 4. DTA results for BMImBF<sub>4</sub>.

### 4.2. NMR Analysis

None of structural changes on heating were revealed (Figure 5). The only effect of temperature change was marked for <sup>11</sup>B. It is a broadening of B1 peak due to increasing of anion motion around cation upon heating. The obtained <sup>1</sup>H spectra are in agreement with those from [32,34–36] and disagree with data from [33]. A possible source of such discrepancy is that, in the latter case, the authors used non-commercial self-synthesized samples and therefore some impurities may not be removed. The theoretical <sup>1</sup>H NMR spectra of [BMIm<sup>+</sup>][BF<sub>4</sub><sup>-</sup>] NIP, imidazol-2-ylidene, and bicyclic IL methyl-4C-imidazolium tetrafluoroborate were obtained by quantum chemical calculations at CAM-B3LYP/aug-cc-pVTZ level of theory. The chemical shift scale was calibrated by tetramethylsilane (TMS). The comparison of theoretical (Figure S2, Supplementary Materials) and experimental spectra corresponds to the structure of [BMIm<sup>+</sup>][BF<sub>4</sub><sup>-</sup>] NIP. The comparison of the obtained <sup>1</sup>H and <sup>13</sup>C spectra with those of imidazole-2-ylidene [10], 1-butylimidazole [49], and 1-methylimidazole [50] indicates the absence of traces of these decomposition products in initial IL.

### 4.3. KEMS

Mass spectrometric experiments were performed in the temperature range of 424–514 K, much below the decomposition temperature (685 K) found by the thermal analysis. The background subtracted mass spectrum recorded at 472 K and the energy of ionizing electrons of 40 eV is shown in Figure 6. In contrast with alkylimidazolium ILs with NTf<sub>2</sub><sup>-</sup> anion [6,13] the obtained mass spectrum has some prominent features. First, the parent cation with  $m/z = 139$  has very low relative intensity; second, the lightweight fragment ions have high intensities with dominating ion with  $m/z = 96$ ; third, the ions with the higher mass than that of the parent cation were also registered ( $m/z = 158, 187$ ).

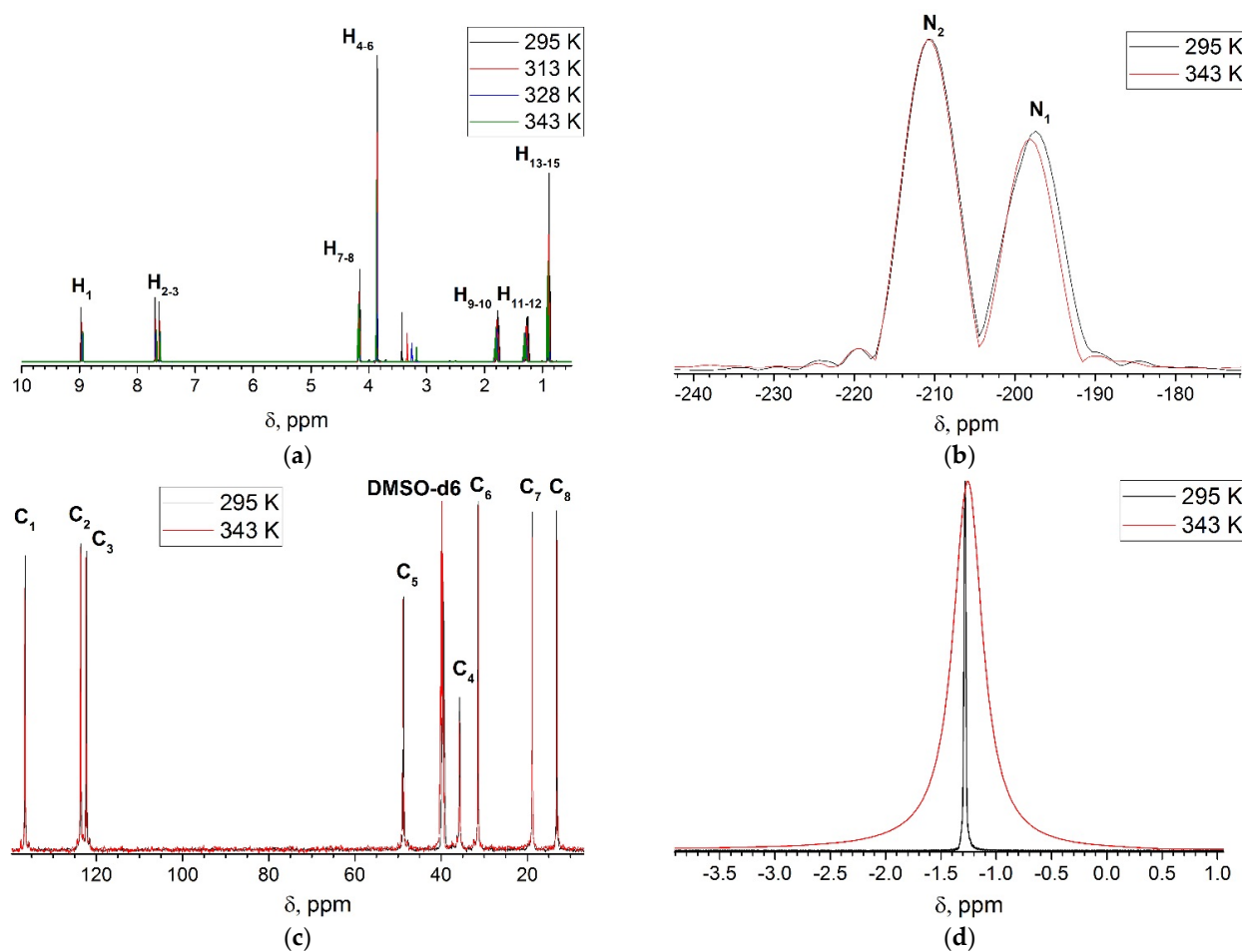


**Figure 5.** NMR spectra of BMImBF<sub>4</sub> at 295–343 K: (a) <sup>1</sup>H; (b) <sup>15</sup>N; (c) <sup>13</sup>C; (d) <sup>11</sup>B. Atom numbering is in accordance with Figure 3.

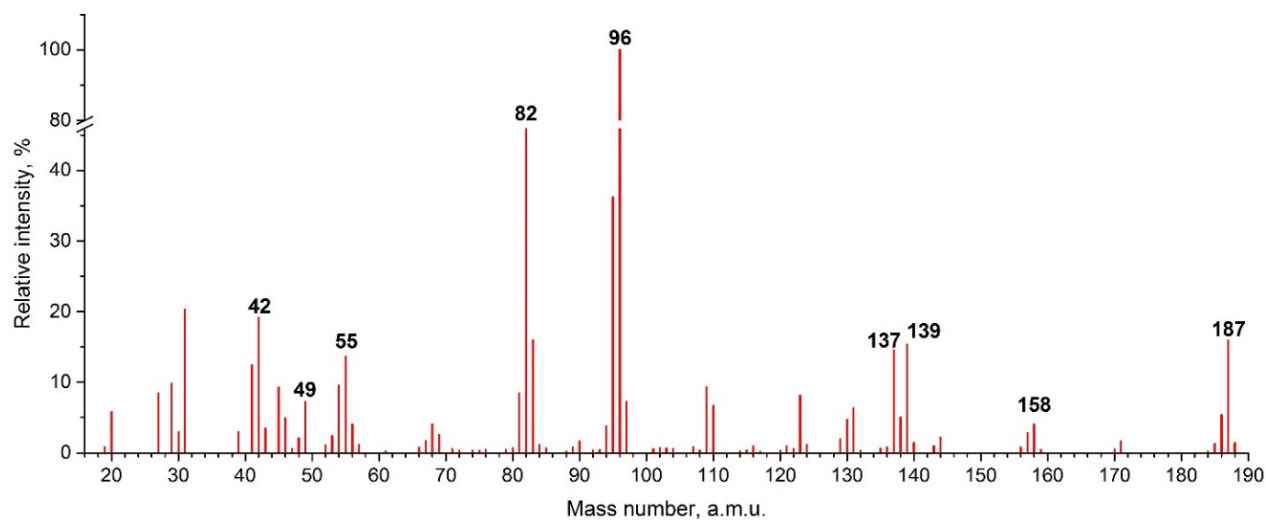


**Figure 6.** EI background subtracted mass spectrum of BMImBF<sub>4</sub> at 472 K.

The temperature dependencies of ion currents in the form  $\ln(IT)$  vs.  $1/T$  and the ionization efficiency curves were measured for the most intense ions (Figure 7). The ion appearance energies ( $AE$ ) obtained from the ionization efficiency curves by a linear extrapolation method together with the slopes of the temperature dependencies are listed in Table 1. The energy scale was calibrated using the background signal of  $\text{HI}^+$  ( $IE(\text{HI}) = 10.38$  eV [51]).

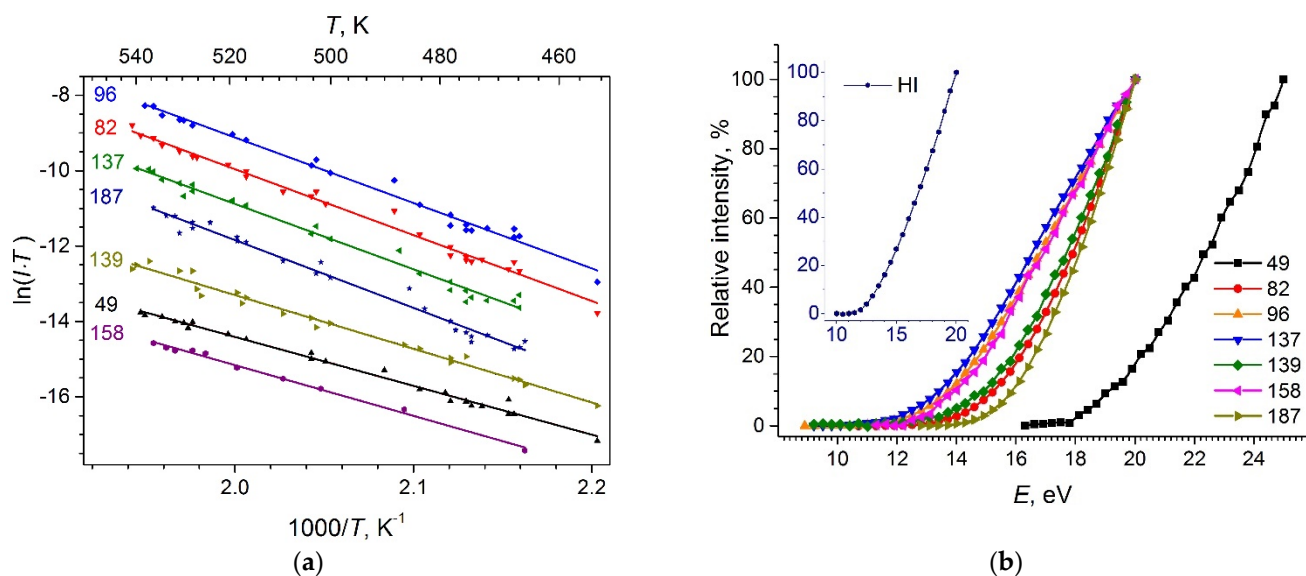


**Figure 7.** Temperature dependencies of ion currents (a) and ionization efficiency curves (b). The intensities of ions with  $m/z = 139$  and  $187$  are scaled by a factor  $0.25$ ;  $m/z = 49$  by  $0.14$ , and  $m/z = 158$  by  $0.11$  to be more illustrative.

**Table 1.** Ion appearance energies  $AE$  and coefficients  $a$  of the  $\ln(I \cdot T) = -1000 \cdot a/T + b$  dependency at  $T = 488$  K.

| $m/z$ | $AE, \text{eV}$ | $a$                | Assigned Ion                          |
|-------|-----------------|--------------------|---------------------------------------|
| 49    | $16.9 \pm 0.5$  | $12.970 \pm 0.274$ | $\text{BF}_2^+$                       |
| 82    | $13.0 \pm 0.5$  | $17.486 \pm 0.364$ | $\text{MIm}^+$                        |
| 96    | $11.3 \pm 0.5$  | $17.365 \pm 0.442$ | $\text{MMIm}^+$                       |
| 137   | $11.0 \pm 0.5$  | $17.327 \pm 0.455$ | $\text{C}_8\text{H}_{13}\text{N}_2^+$ |
| 139   | $12.4 \pm 0.5$  | $14.249 \pm 0.390$ | $\text{BIm}^+$                        |
| 158   | $11.7 \pm 0.5$  | $13.445 \pm 0.363$ | $\text{BImF}^+$                       |
| 187   | $13.8 \pm 0.5$  | $17.968 \pm 0.510$ | $\text{BImBF}_2^+$                    |

A standard uncertainty is given with the “ $\pm$ ” sign.

The temporal dependencies of the ion currents for ions with  $m/z = 82, 96, 137, 139,$  and  $187$  were measured during  $36$  h at  $T = 480$  K and are shown in Figure 8. The ion currents for  $m/z = 96, 137,$  and  $187$  increase in time, the ion current for  $m/z = 82$  is practically time-independent, while the ion current for  $m/z = 139$  decreases in time.

The mass spectrum obtained in this work considerably differs from that in [14]. In the latter work the major peak in mass spectrum was  $m/z = 139$ , with co-dominating  $m/z = 82$ . Despite the ion with  $m/z = 158$  was registered, none of the heavier ions were found. It should be mentioned that the evaporation in [14] was carried out from the open surface in Langmuir conditions while in our work the evaporation was performed in Knudsen conditions.

To clarify the influence of evaporation conditions on vapor composition, the additional experiments on  $\text{BImBF}_4$  evaporation from the open Knudsen cell (intermediate between Knudsen and Langmuir conditions) and from the entirely open surface of IL (Langmuir conditions) were carried out. The recorded mass spectra for the selected peaks are given in Table 2. The mass spectrum from the open surface is very close to that obtained in [14]. The tendency of increasing of the intensity of the parent cation ( $m/z = 139$ ) is observed in

the effusion cell—open cell—open surface series, while the intensity of ions with  $m/z = 82, 96, 137$  decreases in the same series. The ion with  $m/z = 187$  was found only in Knudsen conditions. In work [12] the same effect of the mass spectrum dependence from the area of the effusion orifice was reported for the BMImPF<sub>6</sub>. The changes in the mass spectra at different evaporation conditions for BMImBF<sub>4</sub> and BMImPF<sub>6</sub> are shown in Figure 9. One can see that the behavior of relative intensities is the same for both ILs and strongly depends on a ratio of effusion area to evaporation area.

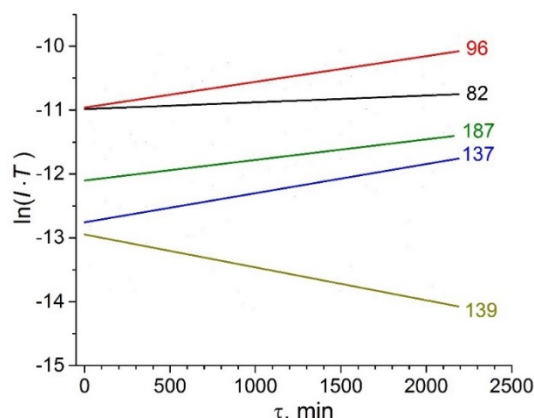


Figure 8. Time dependencies of ion currents at 480 K.

Table 2. Mass spectra of BMImBF<sub>4</sub> recorded at different evaporation conditions.

|                | T, K | m/z |     |     |     |     |     |
|----------------|------|-----|-----|-----|-----|-----|-----|
|                |      | 82  | 96  | 137 | 139 | 158 | 187 |
| Effusion cell  | 487  | 250 | 455 | 95  | 100 | 18  | 68  |
| Open cell      | 470  | 157 | 284 | 63  | 100 | **  | -   |
| Open surface   | 471  | 52  | 52  | 21  | 100 | **  | -   |
| Open surface * | 501  | 44  | 23  | 15  | 100 | 13  | -   |

\*—reproduced as well as possible from Figure 3 in [14]; \*\*—not measured.

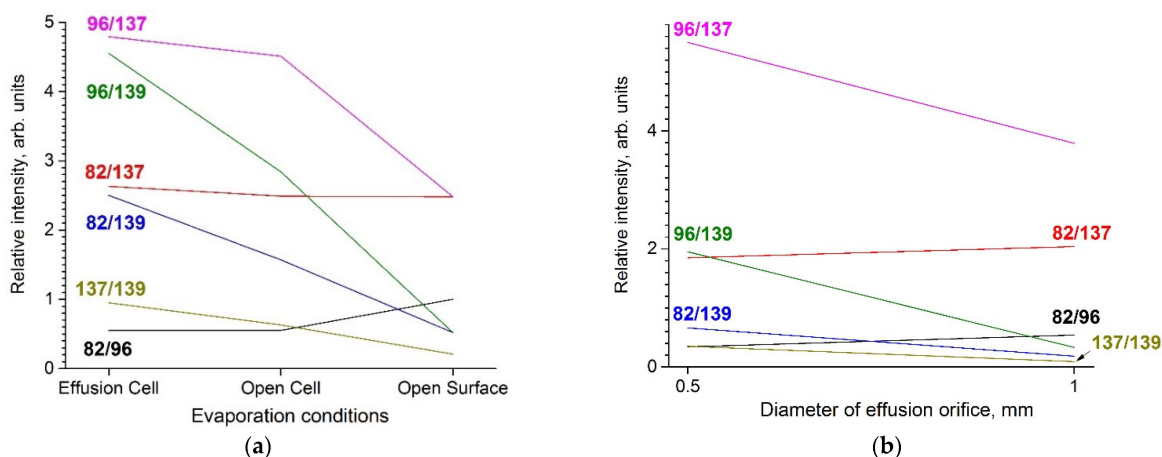
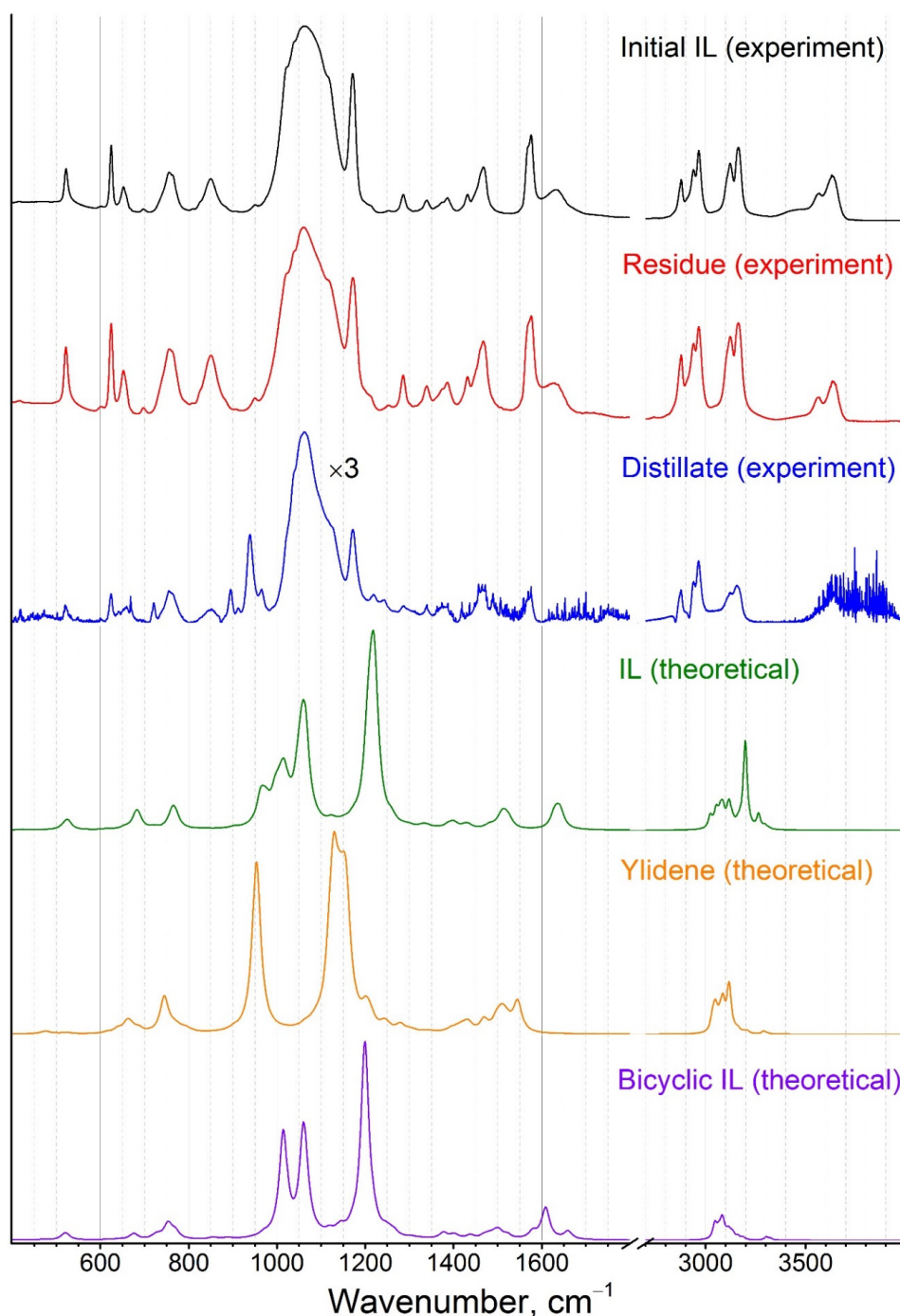


Figure 9. Intensity ratio of ion currents of BMImBF<sub>4</sub> (a) and BMImPF<sub>6</sub> [12] (b).

#### 4.4. IR-Spectroscopy

The IR-spectra (Figure 10) were recorded for the initial IL, the residue after the mass spectrometric experiment, and the distillate collected from the surface of the collimator located in front of the effusion orifice. The analysis of the spectra revealed the absence of any substantial changes in the condensed phase in the Knudsen cell during mass spectrometric experiments, when the sample was heated up to 514 K. However, the IR-spectrum of the

distillate had some distinctive features in 800–1000  $\text{cm}^{-1}$  region. All obtained spectra were identical to those in [17]. To attribute registered peaks in the spectra a quantum chemical modelling of the vibrational spectrum (CAM-B3LYP/cc-pVTZ level of theory) was performed. All theoretical spectra were calculated at 500 K as a combination of those for conformers (18 conformers in the case of BMImBF<sub>4</sub>; 9 for ylidene; two for bicyclic IL) taking into account their mole fractions (Figures 11 and 12).



**Figure 10.** Experimental IR-spectra of condensed phase of BMImBF<sub>4</sub> and theoretical IR-spectra of BMImBF<sub>4</sub>, imidazole-2-ylidene, and bicyclic IL.

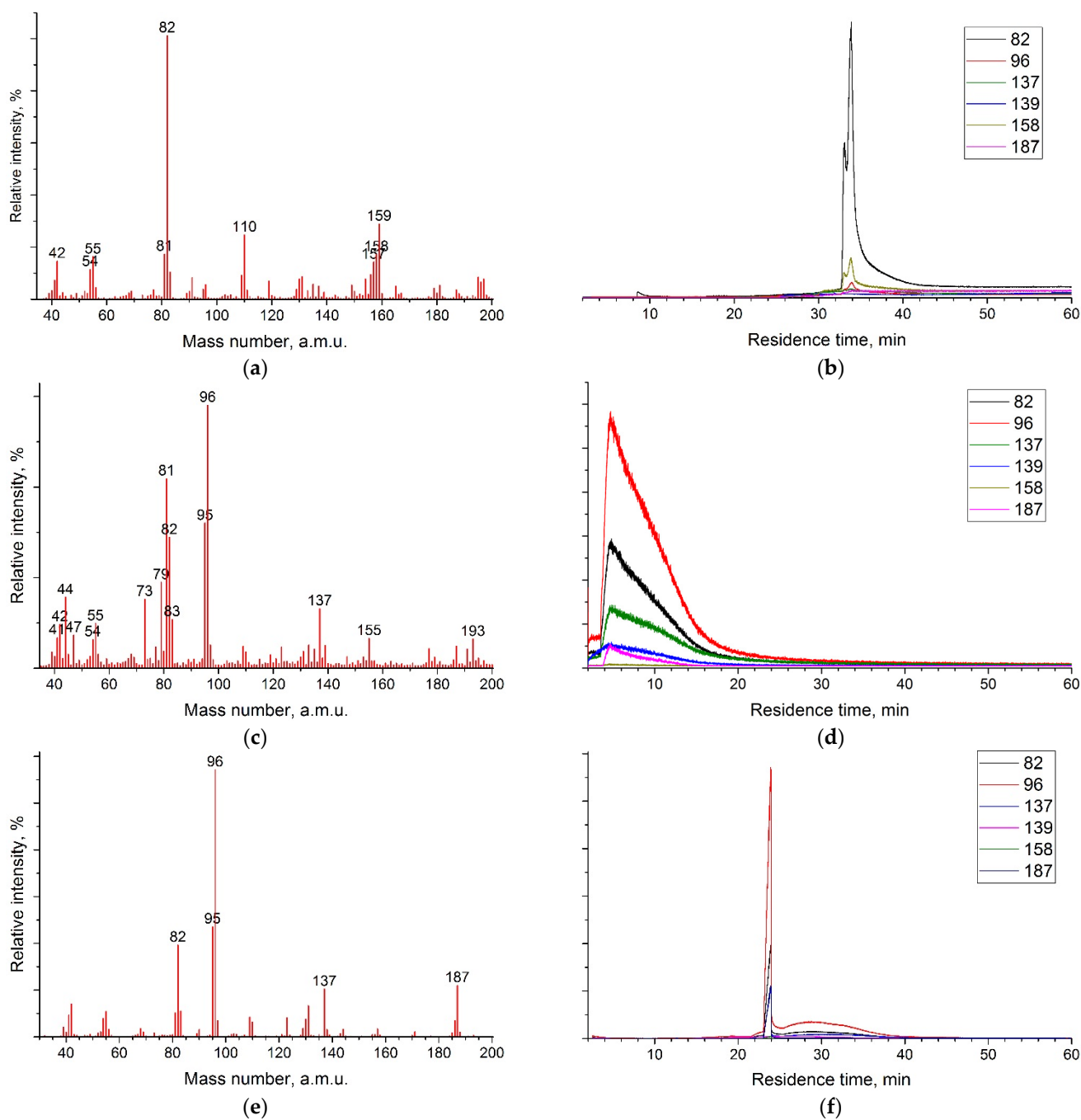


**Figure 11.** GCMS mass spectra and ion profiles on chromatograms of BMImBF<sub>4</sub> with polar (a,b) and nonpolar chromatography column without (c,d) and with (e,f) addition of ethanol.

Comparison of the theoretical and experimental spectra showed that the initial IL as well as the residue after the KEMS experiment consisted of BMImBF<sub>4</sub> whereas the distillate contains imidazole-2-ylidene along with BMImBF<sub>4</sub>.

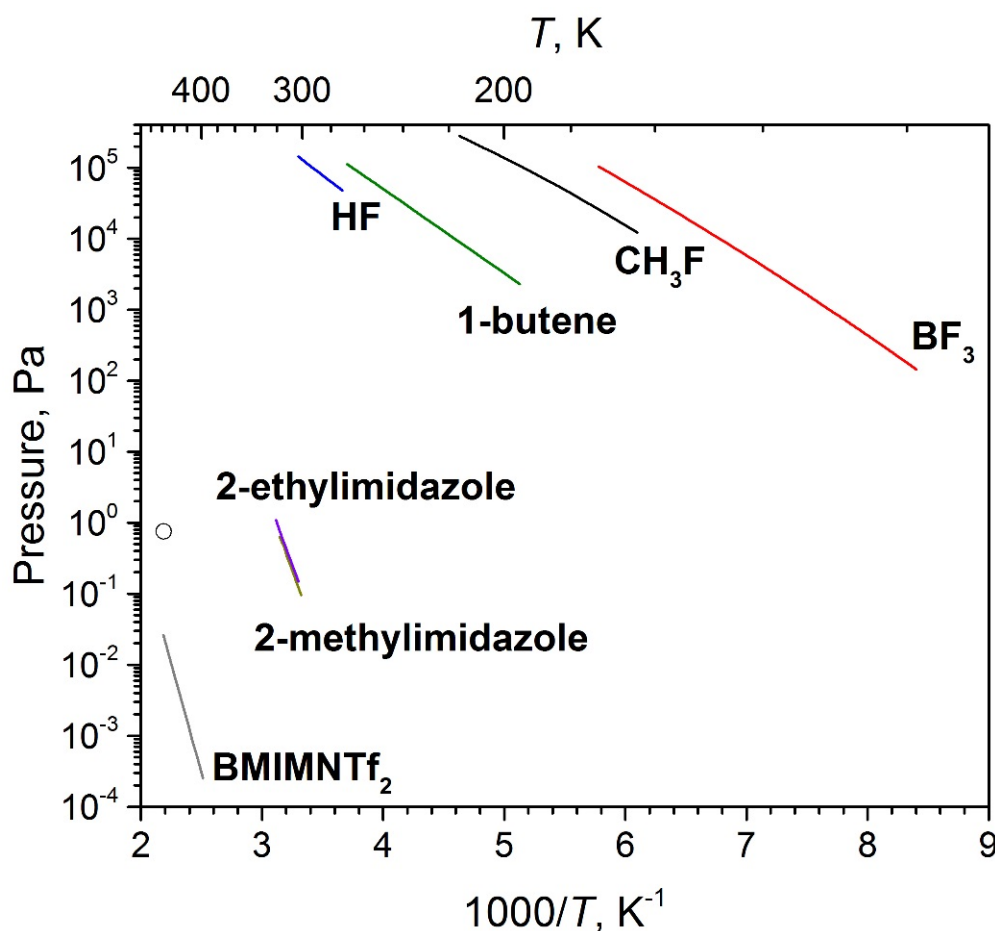


**Figure 12.** Temperature dependencies of vapor pressures of some decomposition products of BMImBF<sub>4</sub>. Temperature dependence of BMImNTf<sub>2</sub> is shown for comparison. Assessed pressure of ylidene was marked as a circle.

#### 4.5. GCMS

The GCMS mass spectra and the ion profiles in BMImBF<sub>4</sub> chromatograms with a polar and nonpolar chromatograph column are shown in Figure 11. The chromatogram profile on the nonpolar column recorded for the pure undiluted IL was rather broadened (Figure 11d). The most likely explanation is an interaction of BMImBF<sub>4</sub> with the column material. The addition of ethanol into the sample results in a peak narrowing (Figure 11f). The only peak on the chromatogram pointed out the presence of a single nonpolar compound in vapor.

The chromatogram recorded on the polar column (Figure 11a) had the only peak as well (despite of a slight splitting both peaks have the same mass spectra). Its mass spectrum is characterized by the dominating ion with  $m/z = 82$  and the sufficiently lower intensity peaks with  $m/z = 159, 110, 55,$  and  $42$ .

#### 5. Discussion

To determine the vapor composition of BMImBF<sub>4</sub> a proper mass spectrum interpretation should be carried out. Molecular precursors of the ions were defined based on the data of the KEMS and GCMS experiments.

The identification of the molecular precursors of the ions was performed on the basis of two principles: (1) the ions from the same molecule usually show close slopes of the temperature dependencies of ion currents, and (2)  $AE$  of fragment ions increases with decreasing their masses. In addition, for experiments on the Knudsen/Langmuir evaporation, the following statement is true: the ratio of ion currents from the same molecule does not depend on the evaporation conditions.

The parent cation with  $m/z = 139$  has  $AE$  ( $12.4 \pm 0.5$  eV), which is consistent with the value from [14] ( $12.8 \pm 0.4$  eV). This  $AE$  value is considerably higher than those obtained for the parent cations of prototypical ILs BMImNTf<sub>2</sub> ( $9.3 \pm 0.3$  eV) [12] and EMImNTf<sub>2</sub> ( $8.9 \pm 0.2$  eV) [52] and at the same time it is closer to the  $AE$  obtained for the similar BMImPF<sub>6</sub> IL ( $11.3 \pm 0.5$  eV) [12]. This fact points out another nature of electron ionization of such class of ILs caused by the stronger cation-anion interaction. As a result, the ion with  $m/z = 158$  corresponding to BMImF<sup>+</sup> has appeared. The scheme of this ion formation suggested in [14] includes the intramolecular rearrangement during ionization.  $AE$  (BMImF<sup>+</sup>/BMImBF<sub>4</sub>) =  $11.7 \pm 0.5$  eV is lower than that of the parent cation. The same situation was observed for origination of BMImF<sup>+</sup> from BMImPF<sub>6</sub> ( $AE$  (BMImF<sup>+</sup>/BMImPF<sub>6</sub>) =  $11.1 \pm 0.3$  eV) [12]. The slopes of temperature dependency of ion current for the ions with  $m/z = 158$  and  $m/z = 139$  are very close (Table 1) indicating the origination of the ion with  $m/z = 158$  directly from NIP. This fact is additionally confirmed by GCMS data on a polar column where the signal with  $m/z = 158$  was detected. An indirect proof of the origin of the ion with  $m/z = 158$  from NIP is the constant ratio 158/139 observed with the different sizes of effusion orifice in the experiment with BMImPF<sub>6</sub> [12].

The ion with  $m/z = 49$  is BF<sub>2</sub><sup>+</sup> having  $AE = 16.9 \pm 0.5$  eV close to  $AE$  (BF<sub>2</sub><sup>+</sup>/BF<sub>3</sub>) =  $16 \pm 1$  eV [53] indicating BF<sub>3</sub> as a possible molecular precursor of this ion. At the same time, the slope of the temperature dependence for an ion with  $m/z = 49$  is similar to that for ions with  $m/z = 139$  and 158 (Table 1). This indicates the second source of origin of the BF<sub>2</sub><sup>+</sup> ion from [BMIm<sup>+</sup>][BF<sub>4</sub><sup>-</sup>] NIP.

The ions with  $m/z = 82, 96, 137,$  and 187 have similar slopes of the temperature dependencies of ion currents. Their  $AE$  values increases in the  $m/z$  series 137-96-82 corresponding to the abovementioned assignment rule. An exception from this rule is the ion with  $m/z = 187$  having the highest appearance energy. However, this circumstance can be explained assuming the different ionization process for this ion. Let us demonstrate it basing on the  $AE$  values of BF<sub>3</sub>. The bond between boron and fluorine is quite strong, even to detach one fluorine atom from boron trifluoride it needs the high energy  $AE$  (BF<sub>2</sub><sup>+</sup>/BF<sub>3</sub>) =  $16 \pm 1$  eV [53]. Therefore, the relatively high  $AE$  value of the ion with  $m/z = 187$  can be explained by the nature of B-F interaction. A similar situation is observed [54] upon ionization of the B<sub>2</sub>F<sub>4</sub> molecule with  $AE$  (BF<sup>+</sup>/B<sub>2</sub>F<sub>4</sub>) <  $AE$  (BF<sub>2</sub><sup>+</sup>/B<sub>2</sub>F<sub>4</sub>) <  $AE$  (B<sub>2</sub>F<sub>3</sub><sup>+</sup>/B<sub>2</sub>F<sub>4</sub>) due to the different processes for the BF<sup>+</sup>, BF<sub>2</sub><sup>+</sup>, and B<sub>2</sub>F<sub>3</sub><sup>+</sup> ions formation including different co-products. The data of KEMS, GCMS and Knudsen/Langmuir evaporation experiments confirmed a single source of the ions with  $m/z = 96, 137,$  and 187. Comparison of the mass spectra obtained for IL by GCMS and KEMS, and by DIMS [10] for imidazole-2-ylidene showed their qualitative similarity (Table 3). Small quantitative differences can be explained by some additional contribution into these signals from NIP in our work and a possible difference in the ion source constructions as well as different types of mass analyzers. Therefore, one can conclude that imidazole-2-ylidene is the main molecular precursor of these ions. Ylidene has no ionic bond and its ionization mechanism is close to those of inorganic polyhalides (see [55]) where the intensity of the molecular ion is less (or absent at all) than that of the first dissociative ion. That is why there is no molecular ion with  $m/z = 206$ , but the ion with  $m/z = 187$  is present in the mass spectrum.

**Table 3.** The relative intensities of four main peaks in mass spectra of BMImBF<sub>4</sub> and imidazole-2-ylidene.

|                        | Compound            | $T, K$ | $m/z$ |     |     |     |
|------------------------|---------------------|--------|-------|-----|-----|-----|
|                        |                     |        | 82    | 96  | 137 | 187 |
| GCMS (nonpolar column) | BMImBF <sub>4</sub> | 523    | 34    | 100 | 18  | 19  |
| KEMS (effusion cell)   | BMImBF <sub>4</sub> | 487    | 55    | 100 | 21  | 15  |
| DIMS [10]              | Imidazole-2-ylidene | 323    | 28    | 100 | 27  | 64  |

The assignment of the ion with  $m/z = 82$  is rather complicated. Analysis of the temperature dependencies of ion currents and the ionization efficiency curves allows us to assign it to the same neutral precursor as for the ions with  $m/z = 96, 137,$  and  $187,$  i.e., to imidazole-2-ylidene. However, according to GCMS data, the ion with  $m/z = 82$  is present in the mass spectrum on both the polar and nonpolar columns. The previous studies [3,4] of ILs with the  $\text{NTf}_2^-$  anion show that the ion with  $m/z = 82$  is common for alkylimidazolium ILs. This ion can also be formed from 1H-imidazoles via routes **b** and **c** (Figure 1). Analysis of possible evaporation routes according to the schemes depicted in Figure 1b,c was performed on the basis of data from the NIST Mass Spectrometry Data Center [56]. A list of the main peaks in mass spectra for various decomposition processes [56] is given in Table 4. According to route **c** (Figure 1) the intensity of the ion with  $m/z = 34$  corresponding to  $\text{CH}_3\text{F}$  should be very strong; the same is expected for the ion with  $m/z = 97$ —the fragment from 1-butylimidazole. However, the KEMS data don't support this assumption. All main peaks corresponding to route **b** were found in the mass spectrum. The presence of ions with  $m/z = 41$  and  $m/z = 42$  in our mass spectrum and their absence in mass spectrum of pure ylidene [10] pointed out the possibility of evaporation of IL by way **b**. Hence the ion with  $m/z = 82$  has at least three sources: ylidene, 1-methylimidazole, and  $\text{BMImBF}_4$ . The most significant results supporting this conclusion were obtained in an isothermal evaporation experiment (Figure 8). The intensity of the ion with  $m/z = 82$  was almost time-independent, while the intensities of ions with  $m/z = 96, 137, 187$  increased in time considerably. However, the growth in the intensity of these ions was accompanied by a rapid decreasing of the parent cation signal ( $m/z = 139$ ). Therefore, one can assume that at the initial stage the ion with  $m/z = 82$  originates from both NIP and decomposition products, but at the end of the isothermal evaporation experiment the decomposition products are the main molecular precursors of this ion.

**Table 4.** List of the main peaks in mass spectra [56] according to different decomposition processes (for a, b, c, and d designations see Figure 1).

| Process   | The Main Peaks with $m/z$          |
|---|------------------------------------|
| $\text{BMImBF}_4(\text{s}) = \text{BMImBF}_4(\text{g})$ | 82, 139, 158                       |
| a   | 82, 96, 137, 187                   |
| b   | 20, 28, 41, 42, 49, 54, 56, 81, 82 |
| c   | 33, 34, 49, 81, 82, 97             |
| d   | 137                                |

The formation of bicyclic IL is not confirmed, because only one peak was registered in the GCMS experiment with a polar column and there were no traces of cyclization in NMR spectra.

To summarize, the vapor over  $\text{BMImBF}_4$  consists of NIPs and decomposition products according to routes **a** and **b**. Most of the previous investigations [17–19] used TGA and IR-spectroscopy to control the condensed phase of  $\text{BMImBF}_4$  and postulated the absence of any significant decomposition. No traces of these products was found from TGA and IR data on the condensed phase in our work. This discrepancy can be explained as follows. Analysis of the reported in literature [57–61] vapor pressures of potential dissociation products of IL under study (Figure 12) shows that they (with the exception of ylidene) are several orders of magnitude higher than those of prototypical IL  $\text{BMImNTf}_2$  [8]. Therefore, at experimental temperatures, these lightweight products cannot accumulate inside the effusion cell and they rapidly evaporate. That is why the IR-spectrum of the residue in an effusion cell is almost identical to that of the initial IL, whereas in the distillate collected from the cold parts of vacuum chamber the peaks attributed to imidazole-2-ylidene increased. The assessed vapor pressure of imidazole-2-ylidene is about one order of magnitude higher than that of IL. It leads to an amount of these vapor species becomes the higher the nearer are the evaporation conditions to equilibrium (closed system).

The differences in vapor composition under Knudsen and Langmuir conditions, as demonstrated in [12], can be explained by the kinetically hindered decomposition of IL. In a closed system (Knudsen cell) the evaporation flux is in equilibrium with the reverse flux from the cell walls. The highly volatile decomposition products accumulate inside the effusion cell and their pressure become considerable. The reverse flux is absent under Langmuir conditions, leading to the decrease in the pressure of the decomposition products, which is limited by the hindered decomposition speed.

## 6. Conclusions

The evaporation of BMImBF<sub>4</sub> IL is characterized by a complex vapor composition which leads to the appearance of atypical ions in its EI mass spectrum at much lower temperatures (424–514 K) than decomposition temperatures obtained by the TGA (685 K) method. Combined analysis of the KEMS, GCMS, NMR, and IR-spectroscopy data together with a thermal analysis and quantum chemical modelling reveal three competing routes of BMImBF<sub>4</sub> evaporation: (1) congruent in the form of NIPs; (2) with decomposition in the form of imidazole-2-ylidene and HF; and (3) with decomposition in the form of 1-methylimidazole, 1-butene, HF, and BF<sub>3</sub>. Two other possible routes of decomposition of BMImBF<sub>4</sub> in the form of bicyclic IL and H<sub>2</sub> as well as 1-butylimidazole, CH<sub>3</sub>F, and BF<sub>3</sub> are found to be negligible. Quantitative analysis of the vapor composition and vaporization thermodynamics will be given in future papers.

The vapor composition of BMImBF<sub>4</sub> strongly depends on the evaporation conditions. Under equilibrium conditions (Knudsen cell), decomposition products prevail in vapor, while under Langmuir conditions (open surface), evaporation in the form of NIP is preferred. Vapor composition is temperature-dependent as well: the amount of [BMIm<sup>+</sup>][BF<sub>4</sub><sup>-</sup>] NIPs relative to that of the decomposition products decreases by about a factor of three in the temperature range from 450 K to 510 K. The main reason for this specific evaporation of BMImBF<sub>4</sub> is a high reactivity of the C1 atom in the imidazole ring, together with the high electronegativity of the anion. Similar peculiarities were observed for BMImPF<sub>6</sub> evaporation and can be expected for all alkylimidazolium ILs with anions like BF<sub>4</sub><sup>-</sup>, PF<sub>6</sub><sup>-</sup>, AsF<sub>6</sub><sup>-</sup>, SCN<sup>-</sup>, etc.

**Supplementary Materials:** The following are available online at <https://www.mdpi.com/article/10.3390/e23111478/s1>, Figure S1: Structures of BMImBF<sub>4</sub> conformers, Figure S2. Experimental and theoretically predicted NMR spectra.

**Author Contributions:** Conceptualization, A.M.D. and V.B.M.; methodology, L.S.K.; software, A.M.D.; validation, A.M.D., V.B.M. and L.S.K.; formal analysis, L.S.K.; investigation, V.B.M.; resources, L.S.K.; data curation, L.S.K.; writing—original draft preparation, A.M.D.; writing—review and editing, V.B.M. and L.S.K.; visualization, A.M.D.; supervision, L.S.K.; project administration, A.M.D.; funding acquisition, A.M.D. All authors have read and agreed to the published version of the manuscript.

**Funding:** This research was funded by Russian Science Foundation, grant number 21-73-00041, and Ministry of Science and Higher Education of Russia, grant number 075-15-2021-671.

**Institutional Review Board Statement:** Not applicable.

**Informed Consent Statement:** Not applicable.

**Data Availability Statement:** The data presented in this study is available in article.

**Acknowledgments:** This work was supported by Russian Science Foundation under grant No. 21-73-00041. The study was carried out using the resources of the Center for Shared Use of Scientific Equipment of the ISUCT (with the support of the Ministry of Science and Higher Education of Russia, grant No. 075-15-2021-671).

**Conflicts of Interest:** The authors declare no conflict of interest.

## References

1. Wasserscheid, P.; Welton, T. (Eds.) *Ionic Liquids in Synthesis*; Wiley-VCH Verlag GmbH & Co. KGaA: Weinheim, Germany, 2002; p. 355.
2. Earle, M.J.; Esperança, J.M.S.S.; Gilea, M.A.; Lopes, J.N.C.; Rebelo, L.P.N.; Magee, J.W.; Seddon, K.R.; Widegren, J.A. The distillation and volatility of ionic liquids. *Nature* **2006**, *439*, 831–834. [[CrossRef](#)]
3. Armstrong, J.P.; Hurst, C.; Jones, R.G.; Licence, P.; Lovelock, K.R.J.; Satterley, C.J.; Villar-Garcia, I.J. Vapourisation of ionic liquids. *Phys. Chem. Chem. Phys.* **2007**, *9*, 982. [[CrossRef](#)] [[PubMed](#)]
4. Leal, J.P.; Esperança, J.M.S.S.; da Piedade, M.E.M.; Lopes, J.N.C.; Rebelo, L.P.N.; Seddon, K.R. The nature of ionic liquids in the gas phase. *J. Phys. Chem. A* **2007**, *111*, 6176–6182. [[CrossRef](#)] [[PubMed](#)]
5. Zaitsau, D.H.; Kabo, G.J.; Strechan, A.A.; Paulechka, Y.U.; Tschersich, A.; Verevkin, S.P.; Heintz, A. Experimental vapor pressures of 1-alkyl-3-methylimidazolium bis(trifluoromethylsulfonyl)imides and a correlation scheme for estimation of vaporization enthalpies of ionic liquids. *J. Phys. Chem. A* **2006**, *110*, 7303. [[CrossRef](#)] [[PubMed](#)]
6. Chilingarov, N.S.; Medvedev, A.A.; Deyko, G.S.; Kustov, L.M.; Chernikova, E.A.; Glukhov, L.M.; Markov, V.Y.; Ioffe, I.N.; Senyavin, V.M.; Polyakova, M.V.; et al. Mass spectrometric studies of 1-ethyl-3-methylimidazolium and 1-propyl-2,3-dimethylimidazolium bis(trifluoromethyl)-sulfonylimides. *Rapid Commun. Mass Spectrom.* **2015**, *29*, 1227–1232. [[CrossRef](#)] [[PubMed](#)]
7. Wang, C.; Luo, H.; Li, H.; Dai, S. Direct UV-spectroscopic measurement of selected ionic-liquid vapors. *Phys. Chem. Chem. Phys.* **2010**, *12*, 7246–7250. [[CrossRef](#)] [[PubMed](#)]
8. Brunetti, B.; Ciccioli, A.; Gigli, G.; Lapi, A.; Misceo, N.; Tanzi, L.; Cipriotti, S.V. Vaporization of the prototypical ionic liquid BMImNTf2 under equilibrium conditions: A multitechnique study. *Phys. Chem. Chem. Phys.* **2014**, *16*, 15653–15661. [[CrossRef](#)] [[PubMed](#)]
9. Dunaev, A.M.; Motalov, V.B.; Kudin, L.S.; Sergeev, D.N.; Akopyan, A.V. Decomposition temperatures, IR and mass spectra of some chiral ionic liquids based on alkylimidazolium. *Russ. Chem. J.* **2017**, *61*, 35–41.
10. Clarke, C.J.; Puttick, S.; Sanderson, T.J.; Taylor, A.W.; Bourne, R.A.; Lovelock, K.R.J.; Licence, P. Thermal stability of dialkylimidazolium tetrafluoroborate and hexafluorophosphate ionic liquids: Ex situ bulk heating to complement in situ mass spectrometry. *Phys. Chem. Chem. Phys.* **2018**, *20*, 16786–16800. [[CrossRef](#)]
11. Chambreau, S.D.; Schenk, A.C.; Sheppard, A.J.; Yandek, G.R.; Vaghjani, G.L.; Maciejewski, J.; Koh, C.J.; Golan, A.; Leone, S.R. Thermal Decomposition Mechanisms of Alkylimidazolium Ionic Liquids with Cyano-Functionalized Anions. *J. Phys. Chem. A* **2014**, *118*, 11119–11132. [[CrossRef](#)] [[PubMed](#)]
12. Volpe, V.; Brunetti, B.; Gigli, G.; Lapi, A.; Cipriotti, S.V.; Ciccioli, A. Toward the Elucidation of the Competing Role of Evaporation and Thermal Decomposition in Ionic Liquids: A Multitechnique Study of the Vaporization Behavior of 1-Butyl-3-methylimidazolium Hexafluorophosphate under Effusion Conditions. *J. Phys. Chem. B* **2017**, *121*, 10382–10393. [[CrossRef](#)] [[PubMed](#)]
13. Dunaev, A.M.; Motalov, V.B.; Kudin, L.S.; Butman, M.F. Molecular and Ionic Composition of Saturated Vapor over EMImNTf2 Ionic Liquid. *J. Mol. Liq.* **2016**, *219*, 599–601. [[CrossRef](#)]
14. Deyko, A.; Lovelock, K.R.J.; Licence, P.; Jones, R.G. The vapour of imidazolium-based ionic liquids: A mass spectrometry study. *Phys. Chem. Chem. Phys.* **2011**, *13*, 16841–16850. [[CrossRef](#)] [[PubMed](#)]
15. Meine, N.; Benedito, F.; Rinaldi, R. Thermal stability of ionic liquids assessed by potentiometric titration. *Green Chem.* **2010**, *12*, 1711–1714. [[CrossRef](#)]
16. Swiderski, K.; McLean, A.; Gordon, C.M.; Vaughana, D.H. Estimates of internal energies of vaporisation of some room temperature ionic liquids. *Chem. Commun.* **2004**, *19*, 2178–2179. [[CrossRef](#)]
17. Zaitsau, D.H.; Yermalayeu, A.V.; Schubert, T.J.S.; Verevkin, S.P. Alkyl-imidazolium tetrafluoroborates: Vapor pressure, thermodynamics of vaporization, and enthalpies of formation. *Mol. Liq.* **2017**, *242*, 951–957. [[CrossRef](#)]
18. Liang, R.; Yang, M.; Zhou, Q. Thermal Stability, Equilibrium Vapor Pressure and Standard Enthalpy of Vaporization of 1-Butyl-3-methylimidazolium Tetrafluoroborate. *Acta Phys.-Chim. Sin.* **2010**, *26*, 1468–1472. [[CrossRef](#)]
19. Krannich, M.; Heym, F.; Jess, A. Characterization of Six Hygroscopic Ionic Liquids with Regard to Their Suitability for Gas Dehydration: Density, Viscosity, Thermal and Oxidative Stability, Vapor Pressure, Diffusion Coefficient, and Activity Coefficient of Water. *J. Chem. Eng. Data* **2016**, *61*, 1162–1176. [[CrossRef](#)]
20. Deyko, A.; Lovelock, K.R.J.; Corfield, J.-A.; Taylor, A.W.; Gooden, P.N.; Villar-Garcia, I.J.; Licence, P.; Jones, R.G.; Krasovskiy, V.G.; Chernikova, E.A.; et al. Measuring and predicting  $\Delta_{\text{vap}}H_{298}$  values of ionic liquids. *Phys. Chem. Chem. Phys.* **2009**, *11*, 8544–8555. [[CrossRef](#)]
21. Lovelock, K.R.J.; Deyko, A.; Licence, P.; Jones, R.G. Vaporisation of an ionic liquid near room temperature. *Phys. Chem. Chem. Phys.* **2010**, *12*, 8893–8901. [[CrossRef](#)] [[PubMed](#)]
22. Deyko, A.; Hessey, S.G.; Licence, P.; Chernikova, E.A.; Krasovskiy, V.G.; Kustov, L.M.; Jones, R.G. The enthalpies of vaporisation of ionic liquids: New measurements and predictions. *Phys. Chem. Chem. Phys.* **2012**, *14*, 3181–3193. [[CrossRef](#)]
23. Fredlake, C.P.; Crosthwaite, J.M.; Hert, D.G.; Aki, S.N.V.K.; Brennecke, J.F. Thermophysical Properties of Imidazolium-Based Ionic Liquids. *J. Chem. Eng. Data* **2004**, *49*, 954–964. [[CrossRef](#)]
24. Ngo, H.L.; LeCompte, K.; Hargens, L.; McEwen, A.B. Thermal properties of imidazolium ionic liquids. *Thermochim. Acta* **2000**, *357*, 97–102. [[CrossRef](#)]

25. Huddleston, J.G.; Visser, A.E.; Reichert, W.M.; Willauer, H.D.; Broker, G.A.; Rogers, R.D. Characterization and comparison of hydrophilic and hydrophobic room temperature ionic liquids incorporating the imidazolium cation. *Green Chem.* **2001**, *3*, 156–164. [[CrossRef](#)]
26. Eapen, T.; Deepthi, T.; Kunduchi, P.V.; Benny, K.G. Mechanistic outlook on thermal degradation of 1,3-dialkyl imidazolium ionic liquids and organoclays. *RSC Adv.* **2016**, *6*, 9421–9428. [[CrossRef](#)]
27. Ohtani, H.; Ishimura, S.; Kumai, M. Thermal decomposition behaviors of imidazolium-type ionic liquids studied by pyrolysis-gas chromatography. *Anal. Sci.* **2008**, *24*, 1335–1340. [[CrossRef](#)] [[PubMed](#)]
28. Arduengo, A.J.; Harlow, R.L.; Kline, M. A stable crystalline carbene. *J. Am. Chem. Soc.* **1991**, *113*, 361–363. [[CrossRef](#)]
29. Taylor, A.W.; Lovelock, K.R.J.; Jones, R.G.; Licence, P. Borane-substituted imidazol-2-ylidenes: Syntheses in vacuo. *Dalton Trans.* **2011**, *40*, 1463–1470. [[CrossRef](#)]
30. Kan, H.; Tsengy, M.; Chu, Y. Bicyclic imidazolium-based ionic liquids: Synthesis and characterization. *Tetrahedron* **2007**, *63*, 1644–1653. [[CrossRef](#)]
31. Knorr, M.; Icker, M.; Efimova, A.; Schmidt, P. Reactivity of Ionic Liquids: Studies on Thermal Decomposition Behavior of 1-Butyl-3-methylimidazolium Tetrafluoroborate. *Thermochim. Acta* **2020**, *694*, 178786. [[CrossRef](#)]
32. Chaudhary, G.R.; Bansal, S.; Mehta, S.K.; Ahluwalia, A.S. Thermophysical and Spectroscopic Studies of Pure 1-Butyl-3-methylimidazolium Tetrafluoroborate and Its Aqueous Mixtures. *J. Solut. Chem.* **2014**, *43*, 340–359. [[CrossRef](#)]
33. Cha, S.; Ao, M.; Sung, W.; Moon, B.; Ahlström, B.; Johansson, P.; Ouchi, Y.; Kim, D. Structures of ionic liquid-water mixtures investigated by IR and NMR spectroscopy. *Phys. Chem. Chem. Phys.* **2014**, *16*, 9591–9601. [[CrossRef](#)]
34. Zheng, Y.-Z.; Wang, N.-N.; Luo, J.-J.; Zhou, Y.; Yu, Z.-W. Hydrogen-bonding interactions between [BMIM][BF<sub>4</sub>] and acetonitrile. *Phys. Chem. Chem. Phys.* **2013**, *15*, 18055–18064. [[CrossRef](#)] [[PubMed](#)]
35. Dharaskar, S.A.; Wasewar, K.L.; Varma, M.N.; Shende, D.Z.; Yoo, C. Synthesis, characterization and application of 1-butyl-3-methylimidazolium tetrafluoroborate for extractive desulfurization of liquid fuel. *Arab. J. Chem.* **2016**, *9*, 578–587. [[CrossRef](#)]
36. Li, Y.; Hu, Y.; Chen, G.; Wang, Z.; Jin, X. Rapid proton diffusion in hydroxyl functionalized imidazolium ionic liquids. *Sci. China Ser. B Chem.* **2017**, *60*, 734–739. [[CrossRef](#)]
37. Dunaev, A.M.; Motalov, V.B.; Kudin, L.S. A High-Temperature Mass-Spectrometric Method for Determination of the Electron Work Function of Ionic Crystals: Lanthanum, Cerium, and Praseodymium Triiodides. *Russ. J. Gen. Chem.* **2017**, *87*, 632–638. [[CrossRef](#)]
38. Dunaev, A.M.; Kryuchkov, A.S.; Kudin, L.S.; Butman, M.F. Automatic complex for high temperature investigation on basis of mass spectrometer MI1201. *Izv. Vyssh. Uchebn. Zaved. Khim. Khim. Tekhnol.* **2011**, *54*, 73–77. (In Russian)
39. Sergeev, D.N.; Dunaev, A.M.; Ivanov, D.A.; Golovkina, Y.A.; Gusev, G.I. Automatization of mass spectrometer for the obtaining of ionization efficiency functions. *Prib. Tekhnika Eksperimenta* **2014**, *1*, 139–140. (In Russian) [[CrossRef](#)]
40. Grimme, S.; Antony, J.; Ehrlich, S.; Krieg, H. A consistent and accurate ab initio parameterization of density functional dispersion correction (DFT-D) for the 94 elements H-Pu. *J. Chem. Phys.* **2010**, *132*, 154104. [[CrossRef](#)]
41. Yanai, T.; Tew, D.P.; Handy, N.C. A new hybrid exchange-correlation functional using the Coulomb-attenuating method (CAM-B3LYP). *Chem. Phys. Lett.* **2004**, *393*, 51–57. [[CrossRef](#)]
42. Zhao, Y.; Truhlar, D.G. The M06 suite of density functionals for main group thermochemistry, thermochemical kinetics, noncovalent interactions, excited states, and transition elements: Two new functionals and systematic testing of four M06-class functionals and 12 other functionals. *Theor. Chem. Acc.* **2008**, *120*, 215–241. [[CrossRef](#)]
43. Dunning, J. Gaussian basis sets for use in correlated molecular calculations. I. The atoms boron through neon and hydrogen. *J. Chem. Phys.* **1989**, *90*, 1007–1023. [[CrossRef](#)]
44. Frisch, M.J.; Trucks, G.W.; Schlegel, H.B.; Scuseria, G.E.; Robb, M.A.; Cheeseman, J.R.; Scalmani, G.; Barone, V.; Mennucci, B.; Petersson, G.A.; et al. *Gaussian 09, Revision D.02*; Gaussian Inc.: Wallingford, CT, USA, 2009.
45. van Valkenburg, M.E.; Vaughn, R.L.; Williams, M.; Wilkes, J.S. Thermochemistry of ionic liquid heat-transfer fluids. *Thermochim. Acta* **2005**, *425*, 181–188. [[CrossRef](#)]
46. Schreiner, C. Synthese und Charakterisierung neuer Ionischer Flüssigkeiten auf der Basis gemischter Fluorborat-Anionen. Ph.D. Thesis, University of Regensburg, Regensburg, Germany, 2009.
47. Holbrey, J.D.; Seddon, K.R. The phase behaviour of 1-alkyl-3-methylimidazolium tetrafluoroborates; ionic liquids and ionic liquid crystals. *Chem. Soc. Dalton Trans.* **1999**, 2133–2140. [[CrossRef](#)]
48. Erdmenger, T.; Vitz, J.; Wiesbrock, F.; Schubert, U.S. Influence of different branched alkyl side chains on the properties of imidazolium-based ionic liquids. *J. Mater. Chem.* **2008**, *18*, 5267–5273. [[CrossRef](#)]
49. Hog, M.; Schneider, M.; Studer, G.; Bäuerle, M.; Föhrenbacher, S.A.; Scherer, H.; Krossing, I. An Investigation of the Symmetric and Asymmetric Cleavage Products in the System Aluminum Trihalide/1-Butylimidazole. *Chem. A Eur. J.* **2017**, *23*, 11054–11066. [[CrossRef](#)] [[PubMed](#)]
50. Pachler, K.G.R.; Pachter, R.; Wessels, P.L. Carbon-13proton coupling constants in N-substituted imidazoles. A <sup>13</sup>C NMR study and MO calculations. *Magn. Reson. Chem.* **1981**, *17*, 278–284. [[CrossRef](#)]
51. Kimura, K.; Katsumata, S.; Achiba, Y.; Yamazaki, T.; Iwata, S. Ionization energies, Ab initio assignments, and valence electronic structure for 200 molecules. In *Handbook of HeI Photoelectron Spectra of Fundamental Organic Compounds*; Japan Scientific Societies Press: Tokyo, Japan, 1981; p. 268.

52. Strasser, D.; Goulay, F.; Kelkar, M.S.; Maginn, E.J.; Leone, S.R. Photoelectron Spectrum of Isolated Ion-Pairs in Ionic Liquid Vapor. *J. Phys. Chem. A* **2007**, *111*, 3191–3195. [[CrossRef](#)]
53. Farber, M.; Srivastava, R.D.; Moyer, J.W. Mass spectrometric determination of the thermodynamics of potassium hydroxide and minor potassium-containing species required in magnetohydrodynamic power systems. *J. Chem. Thermodyn.* **1982**, *14*, 1103–1113. [[CrossRef](#)]
54. Dibeler, V.H.; Liston, S.K. Mass-spectrometric study of photoionization. XII. Boron trifluoride and diboron tetrafluoride. *Inorg. Chem.* **1968**, *7*, 1742–1746. [[CrossRef](#)]
55. Pogrebnoi, A.M.; Kudin, L.S.; Motalov, V.B.; Goryushkin, V.F. Vapor species over cerium and samarium trichlorides, enthalpies of formation of (LnCl<sub>3</sub>)<sub>n</sub> molecules and Cl–(LnCl<sub>3</sub>)<sub>n</sub> ions. *Rapid Commun. Mass Spectrom.* **2001**, *15*, 1662–1671. [[CrossRef](#)] [[PubMed](#)]
56. Acree, W.E., Jr.; Chickos, J.S. *NIST Chemistry WebBook, NIST Standard Reference Database Number 69*; Linstrom, P.J., Mallard, W.G., Eds.; National Institute of Standards and Technology: Gaithersburg, MD, USA, 1998; p. 20899. [[CrossRef](#)]
57. Stull, D.R. Vapor Pressure of Pure Substances. Organic and Inorganic Compounds. *Ind. Eng. Chem.* **1947**, *39*, 517–540. [[CrossRef](#)]
58. Sheft, I.; Perkins, A.J.; Hyman, H.H. Anhydrous Hydrogen Fluoride: Vapor Pressure and Liquid Density. *J. Inorg. Nucl. Chem.* **1973**, *35*, 3677–3680. [[CrossRef](#)]
59. Michels, A.; Wassenaar, T. Vapour pressure of methylfluoride. *Physica* **1948**, *14*, 104–110. [[CrossRef](#)]
60. Coffin, C.C.; Maass, O. The Preparation and Physical Properties of  $\alpha$ -,  $\beta$ - and  $\gamma$ -Butylene and Normal and Isobutane. *J. Am. Chem. Soc.* **1928**, *50*, 1427–1437. [[CrossRef](#)]
61. Jiménez, P.; Roux, M.V.; Turrión, C. Thermochemical properties of N-heterocyclic compounds IV. Enthalpies of combustion, vapour pressures and enthalpies of sublimation, and enthalpies of formation of 2-methylimidazole and 2-ethylimidazole. *J. Chem. Thermodyn.* **1992**, *24*, 1145–1149. [[CrossRef](#)]